Available online at www.sciencedirect.com
ScienceDirect
Applied Catalysis A: General 313 (2006) 177–188
APPLIED CATALYSIS A: GENERAL
www.elsevier.com/locate/apcata

Sunflower oil hydrogenation on Pd/Al_2O_3 catalysts in single-phase conditions using supercritical propane

C. Piqueras *, S. Bottini, D. Damiani

PLAPIQUI (UNS-CONICET), Camino La Carrindanga km 7, CC 717, CP 8000, Bahía Blanca, Argentina

Received 9 May 2006; received in revised form 19 July 2006; accepted 22 July 2006

Abstract

Several Pd catalysts were prepared on α and γ alumina using palladium acetylacetonate and palladium nitrate as a precursor. The characterization of these catalysts by H_2 chemisorption, XRD and TEM microscopy confirm the presence of different dispersed metallic particles from 1.9 to 12.1 nm. These catalysts were tested in the sunflower oil hydrogenation under supercritical conditions using propane as solvent and 5% mol of hydrogen concentration. The well-known Weisz–Prater criterion was used to determine the extent of mass transport phenomena. While hydrogen mass transport was found free from limitations, oil transport had limitations in some experiments. The reaction is moderately structure sensitive since the turnover number decreases 3 times as the exposed metal percentage (metal dispersion) increases from 9 to 60%. An influence on the selectivities to *trans* isomers, monounsaturated and saturated fatty acids was found when the metallic particle size was decreased. These results are explained by the high adsorption strength of the high-unsaturated fatty acids onto the small particles and the promotion of a ''shunt'' reaction from linoleic to saturated compounds.

Keywords: Hydrogenation; Sunflower oil; Propane; Supercritical fluid

1. Introduction

The oil hydrogenation is a very important process in the food industry. The conventional hydrogenation is usually carried out in stirred batch reactors, where a catalyst powder is intimately put in contact with the gas–liquid mixture. In this type of process, the gas–liquid–solid reaction is controlled by the availability of hydrogen at the catalyst surface, which is limited by both, the low solubility of hydrogen and the high mass transfer resistance of the liquid phase [1]. In this hand, the catalyst efficiency is lowered. The hydrogen scarcity favors the double bond transposition and the *cis–trans* isomerization [2]. This shortness links the external variables (e.g., temperature, stirring rate and hydrogen pressure) with the process selectivity [3].

There is increasing concern and evidence that *trans* fatty acids are harmful to human health [4,5]. Therefore, the development of technologies to minimize the production of *trans* isomerization during hydrogenation is of current interest. Experts in human nutrition recommend that food manufacturers should reduce the levels of *trans* fatty acids produced during hydrogenation [6]. The incentives for manufacturers to do so are becoming more compelling as stricter labelling, requirements and nutritional claims are introduced.

The catalyst development is a field where there have been major advances in this topic. In this way, several catalysts were tested [7–9] to modify the *cis–trans* selectivity, but the reactions seem to be insensitive to the metal morphology. Some authors demonstrated that the hydrogenation rate and selectivity fatty acid ethyl ester are insensitive to the metal particle size and the support nature [10]. Although they concluded that larger metal particle size favors the *cis–trans* isomerizations, the experimental data that support this hypothesis were not conclusive. Other authors [11] did not notice better results in the *cis–trans* selectivity of the reaction, when several transition elements modified the active metal (Pd). They observed a promoting effect of Mo, but no favorable differences in selectivity. Several alternatives such as combined homogeneous and heterogeneous catalysts were evaluated [12]. In this case, activities of catalysts with Ni/Ru mixtures were higher than the activities of the catalysts used individually. Low levels of *trans* isomers (≅15% at IV = 60), characteristic of the Ru catalyst, were also observed.

* Corresponding author. Tel.: +54 291 4861700; fax: +54 291 4861600.
E-mail address: cpiqueras@plapiqui.edu.ar (C. Piqueras).

0926-860X/$ – see front matter © 2006 Elsevier B.V. All rights reserved.
doi:10.1016/j.apcata.2006.07.023

The hydrogenation of liquid substrates with heterogeneous catalysts is diffusion controlled. The use of supercritical fluids reduces this controlling step by elimination of the gas–liquid interface. A supercritical fluid has excellent transport properties that favor the diffusivity of reactants and products. Furthermore, its solvent power can be tuned with the pressure inducing liquid-like solvent behavior [13].

The use of an adequate supercritical fluid can bring the reactive mixture into a homogeneous condition, increasing the rate to gas-like reaction rates. Several authors found reaction rates roughly 500 times higher than in traditional batch reactions in the fatty acid methyl esters hydrogenation [14–16]. While gas–liquid hydrogenation reactions require high temperatures to increase the hydrogen solubility; the temperature of the supercritical process can be modified without effects in compositions. This last result is because of the external variables, which might be uncoupled. In addition, better selectivity to the *cis* isomers can be achieved because the hydrogen concentration may be freely handled. Consequently, isomerization reactions favored by the lack of hydrogen at the catalyst surface can also be diminished, reaching low *trans* isomer levels. Macher reaches around 4% of *trans* isomer concentration in the hydrogenation of palm oil [15].

In the present work, several Pd-Al_2O_3 catalysts with different metal particle size and various Al_2O_3 support were tested. Using propane as supercritical solvent, the reactions were carried out in a homogeneous phase searching for better *cis* isomers selectivity and looking for a possible structure sensitivity of the reaction.

2. Experimental

2.1. Materials

Propane (99.01% molar) provided by TGS, Bahía Blanca, Argentina, was used as the reaction solvent. Chromatographic-grade (99.999% molar) hydrogen, chromatographic-grade (99.999% molar) nitrogen, analytic-grade (99.99% molar) air, argon, and helium (5.0 ultra-pure grade), were provided by AGA, Argentina. The sunflower oil was a refined, bleached, and deodorized commercial one, with initial fatty acids composition 7.94% C16.0 (palmitic), 4.22% C18.0 (stearic), 23.06% C18.1 (oleic), 64.44% C18.2 (linoleic), 0.17% C18.3 (linolenic), 0.54% C20.0 (eicosanoic), 0.64% C22.0 (docosanoic), maintained in inert atmosphere and used without previous treatment. The supports were γ-Al_2O_3 (Condea, Puralox, 148 $m^2\,g^{-1}$) and α-Al_2O_3 (Rhône-Poulenc, 9 $m^2\,g^{-1}$). The metal precursors were $Pd(C_5H_7O_2)_2$, which was provided by Alpha, and $Pd(NO_3)_2$, which was supplied by Sigma.

2.2. Catalyst preparations and characterization

A set of four catalysts was prepared by wet impregnation method with two Al_2O_3 supports and different metal precursors. The Pd-GA catalyst was prepared by impregnation of the γ-Al_2O_3 support with a solution of $Pd(C_5H_7O_2)_2$ in toluene, using an impregnation volume amounting to 5 times the total pore volume. The solution had a Pd concentration equal to 1.1 times the Pd concentration required to leave a nominal loading of 1% Pd content on the support. After impregnation, the catalyst was dried at room temperature for 72 h, then in an Ar atmosphere at 423 K for 2 h and finally, calcined in a flow (100 cm^3/min) of chromatographic air at 673 K for 2 h. Pd-GN catalyst was prepared by incipient wetness method, using $Pd(NO_3)_2$ as a metal precursor. The support was slowly contacted with the impregnating solution. The Pd concentration was adjusted in order to result in a metal loading of 1% (w/w) on the support. The catalysts were dried for 24 h at room temperature; afterwards they were calcined for 2 h at 773 K in chromatographic air. A Pd-GNR catalyst was prepared on the basis of Pd-GN after a reducing treatment in H_2 heating the sample at a 5 K/min rate from 298 to 573 K and allowing the sample to remain at this final temperature during 1 h. This treatment produces a sintering of the Pd clusters [17]. Pd-AA and Pd-AN catalysts were prepared as Pd-GA and Pd-GN, respectively, using α-Al_2O_3 and with the same precursors.

The metal content was determined by atomic absorption spectrometry (Instrumentation Laboratory 551), employing an air–acetylene burner and a Pd-cathode hollow lamp unit. Specific surface areas were evaluated making use of the BET method on a volumetric system Nova 1200e Quantachrome Instruments, utilizing nitrogen as adsorbing gas at 77 K. X-ray diffraction (XRD) patterns were recorded, by means of the powder method, with a PHILIPS PW1710 diffractometer using Cu Kα radiation (45 kV, 30 mA) and a graphite curved monochromator. The 2θ range of 5–70° was scanned at a step size of 0.035° s^{-1}. The H_2 chemisorption uptakes were measured in a conventional glass apparatus [18]. Before reduction, the catalysts were oxidized in air at 773 K during an hour. Then, the samples were purged in He and reduced at 523 K in flowing H_2 for 1 h. Following the reduction, the samples were evacuated for 2 h at reduction temperature and cooled to adsorption temperature (298 K) under vacuum. Irreversible hydrogen uptakes were determined from dual isotherms measured for hydrogen using Benson et al.'s double-isotherm method [19]. The fraction of exposed palladium was calculated assuming a 1:1 hydrogen atom adsorbed per surface palladium atom stoichiometry.

IR of adsorbed CO was recorded on a Nicolet 20DXB spectrometer with a resolution of 4 cm^{-1}. A stainless-steel cell with CaF2 windows connected to a vacuum system was used, wherein the catalyst could be heated under H_2 or He and small pressures of CO could be dosed.

The particle size distribution was determined by transmission electron microscopy (TEM) using a Joel 100 CX instrument operated at 100 kV (Centro Regional de Investigaciones Basicas y Aplicadas de Bahía Blanca). The Pd catalysts were ground and dispersed onto holey carbon-coated Cu grids for direct observation. Over 100 particles were examined on the TEM micrographs and the particle size was calculated according to Eq. (1).

$$d[\mathrm{nm}] = \frac{\sum n_i \mathrm{d}_i^3}{\sum n_i \mathrm{d}_i^2} \quad (1)$$

2.3. High-pressure reactor system

All sets of reactions were carried out in a variable-volume batch cell described elsewhere [20]. The cell's bore is 95.5 mm long and has a diameter of 19.05 mm. The movable piston's length is 25.4 mm, so the total variable volume (excluding the piston volume) is 18.6 cm^3. The cell consists of three parts: a window cap, the cell body, and an end cap. A sapphire window (2.7 cm thick) is attached to the cell body with a window cap. TEFLON O-rings are used for sealing purposes at both ends of the cell. An additional TEFLON O-ring was added to the original design in front of the cell body, to improve the seal at the sapphire window extreme. The movable piston made of stainless steel inserts covered with aluminum to prevent it from scratching the highly polished surface of the bore. The piston has two TEFLON O-rings with a diameter regulating system to generate a pre-charge pressure and thus to prevent the pressurizing fluid from leaking into the cell's window side. This system was tested with a hydrogen/propane (50/50) mixture up to 250 bar at 373 K.

The cell is installed in a nitrogen-purged oven (Bemco Inc.) that is equipped with a fan to ensure uniform temperature. The oven can be controlled within ± 0.1 K. The cell temperature is measured with a platinum resistance thermometer inserted into a thermal well inside the cell body, the error being within ±0.l K. The pressure is measured with a pressure transducer (Heise Model 623) and with an absolute error of ±0.3 bar. The pressure readings are checked against a dial gauge (Heise Model CM). The propane is charged to the cell with a pressure pump (type Ruska Corporation Model 2250) maintained at 293 K, equipped with a refrigerated bath system. This pump allows for an accurate volume reading, and is also used as a pressure generator. In addition, another pressure pump (High Pressure Equipment Co. Model; 62-6-10) is used with sunflower oil as a pressurizing fluid. The hydrogen cylinder was directly connected to the system through a Matheson 3064 S high-pressure regulator and an Asshcrof dial gauge.

The sampling line (0.254-mm, i.d.) allows for taking samples from the middle of the batch cell. This line is heat traced and maintained at the same temperature as the cell. The samples are rapidly depressurized upon switching zero-volume sampling valves (Valco Inc., six-way CW series) and collected in Eppendorf sample flasks.

2.4. Catalytic studies

The cell was charged with the exact amount of sunflower oil determined as the weight difference between the empty cell and the cell loaded with oil, measured in a six-digit scale (Ohaus model Adventure). Then, the cell was sealed and repeatedly filled with hydrogen pulses of 0.2 MPa in pressure and evacuated. Through the hydrogen line, a precise hydrogen mole amount was charged taking into account the free volume of the cell and the dissolved moles in the sunflower oil at a given hydrogen pressure [21]. At this point, an exact amount of liquid propane was charged from a measured angular movement of the pressure pump, which was maintained at constant temperature. A maximum total error of 3% in the composition of the components was found in the loading procedure. Ten to fifteen milligrams of Pd catalysts were used in the reactions. The catalyst was reduced in flowing hydrogen (75 cm^3/min) at 403 K during 1 h. After that, the catalyst was covered with hydrogenated sunflower oil (IV = 50) to prevent the contact with oxygen, and in order to achieve better handling. In this form it was added to the cell.

The reactive mixture was pressurized to reach the homogeneous condition, and then, a temperature ramp was applied (5 K/min) to get the reaction conditions. The global molar compositions for all cases were the following: 5% hydrogen/92.5% propane/2.5% of sunflower oil (SO), and the total volume, considering as the sum of the volume of each pure components, was 24.986 cm^3 at 293.15 K and 78.9 bar, which are the loading conditions. The time was recorded from the beginning of the heating process, but a sample was taken when the temperature was 373 K, and considering the zero run time.

The sample line was purged twice prior to actual sampling, which was tested to be sufficient to clear the line completely. Each time that a sample was withdrawn, the pressure was reestablished with a manual increase through a piston movement, to avoid undesirable liquid phase split. The total volume of the sampling line and the valve was estimated to be about 0.128 cm^3. Seven samples were withdrawn, which represent an 11% of the total volume of the reaction mixture. The samples were analyzed by capillary gas chromatography using a Hewlett Packard 4890 chromatograph with a Supelco SP-2560 chromatographic column. The fatty acid composition was determined following the AOCS Ce 1c-89 norm, which allows the distinction between *cis* and *trans* geometrical isomers. The H_2 conversion was calculated considering the initial moles placed and measuring the degree of saturation of each oil sample that is equal to the moles of H_2 consumed during the reaction. Peaks were assigned according to Sulpelco 37 Component FAME Mix standard (Cat. Number 47885-U).

3. Results and discussion

3.1. H_2-C_3H_8-sunflower oil phase equilibria

In order to search for homogeneous fluid conditions of the reactive mixture, it is necessary to know the phase boundaries of a multicomponent system containing the supercritical solvent, the substrate to be hydrogenated, hydrogen and the reaction products. In the particular case of the hydrogenation of vegetable oils, the initial and final products of the reaction have similar chemical nature; i.e., they are basically high molecular weight triglycerides, differing only in the degree of unsaturation. Therefore, it is expected that the phase boundaries of a ternary system containing hydrogen, propane and a model triglyceride will be representative of the real reactive system [22].

An analysis of the phase behavior of the corresponding binary mixtures helps to understand and estimate the phase limits of the ternary system. The solubility of hydrogen in liquid organic compounds, like alkanes and triglycerides, is low and it increases

with temperature and pressure [23]. The solubility of hydrogen in liquid propane is also low, but both components are completely miscible if the temperature is above the critical temperature of propane. High molecular weight triglycerides have three long hydrocarbon chains that lead to a paraffinic behavior. For this reason, the phase behavior of the binary propane + triglyceride is similar to that of propane + long chain alkanes [23,24]. These systems present a Type V phase diagram in the classification of van Konynenburg and Scott [25,26], with the appearance of liquid–liquid immiscibility and liquid–liquid–vapor locus at temperatures close to the critical temperature of propane. For example, for propane + tripalmitin the liquid–liquid–vapor line extends from 349 K (lower critical end point) to 370 K (upper critical end point) [27].

At temperatures higher than the critical temperature of propane and at pressures above the region of partial miscibility of the binary propane-triglyceride, the ternary system (hydrogen–propane–triglyceride) has only one partially miscible pair (hydrogen + triglyceride) and it is possible to reach homogeneous conditions at high propane concentrations [28]. Fig. 1 shows a schematic phase diagram of the ternary system (hydrogen + propane + SO) derived from the corresponding P–x binary diagrams at a temperature above the critical temperature of propane (T_c = 369.8 K, P_c = 42.48 bar). Hydrogen and propane are completely miscible. At pressure P_1 (Fig. 1(a)) the binary H_2 + SO is at vapor–liquid equilibrium conditions, while the binary propane + SO is under liquid–liquid equilibrium. At this pressure, the ternary system presents two narrow one-phase regions separated by a wide heterogeneous area that includes vapor–liquid, liquid–liquid and vapor–liquid–liquid equilibria. By increasing pressure, the liquid–liquid immiscibility between propane and sunflower oil can be surpassed. At pressure P_2 (Fig. 1(b)) both components are completely miscible and the ternary system presents a homogeneous region at high propane concentrations, where hydrogen and sunflower oil are completely miscible at all proportions. The dashed line in Fig. 1(c) represents the minimum concentration of propane ($x C_3H_8$min = 0.913) required to assure homogeneity of the reaction mixtures at any ratio H_2/SO [22,29]. The black zone to the right of the dashed line indicates the adequate working region for the supercritical hydrogenation process. This is delimited by the minimum molar ratio required by the reaction (H_2/SO = 2) and the minimum solvent molar composition necessary to carry out the reaction without crossing the biphasic region when the reaction takes place.

Therefore, knowledge of the one-phase boundaries and careful control of temperature, pressure and composition are required in order to assure homogeneous hydrogenation conditions.

3.2. Predictive tools

In the present work, the phase equilibrium boundaries were predicted with a group-contribution equation of state GC-EOS [30]. Group-contribution methods are suitable for modeling fatty oil mixtures because the natural oil can be represented by a pseudo-triglyceride molecule containing fatty chains with a number of carbon atoms and double bonds representative of the average molecular weight and degree of unsaturation of the real multicomponent oil. This model has shown to give very good

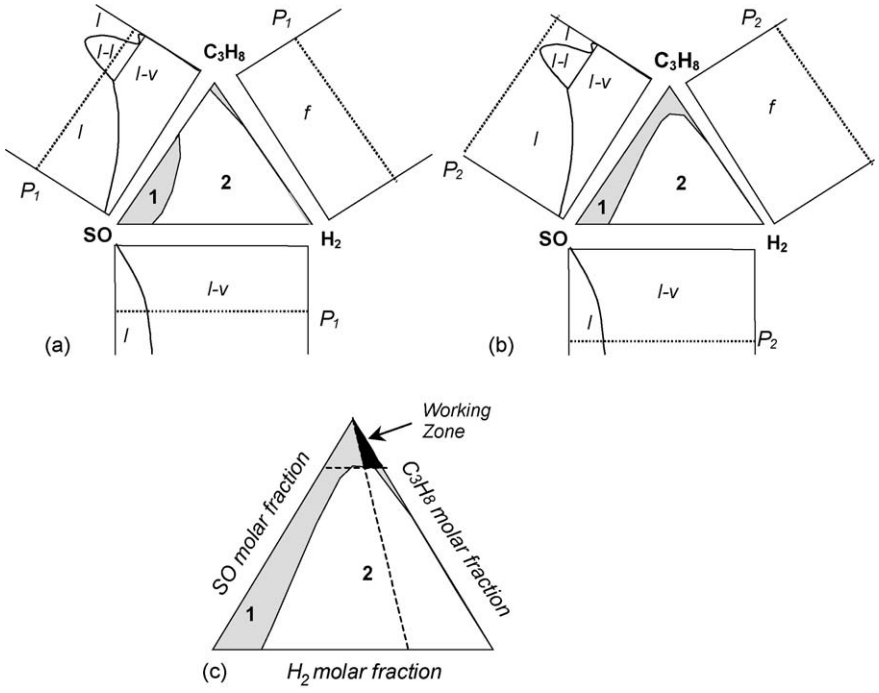

Fig. 1. Schematic ternary Gibbs phase diagrams derived from the corresponding P–x binaries. (1) Homogeneous region; (2) heterogeneous region. (a) At 373.15 K and pressure P_1 (e.g., 10 MPa), there is liquid–liquid and vapor–liquid equilibrium in the binaries (propane-SO and H_2-SO, respectively). (b) At P_2 (e.g., 16.2 MPa) > P_1, the liquid–liquid phase split between propane and SO disappears. (c) Adequate working region for the homogeneous hydrogenation of sunflower oil (373.15 K, 160 bar), $x C_3H_8$min = 0.913, minimum propane molar fraction to work in homogeneous phase.

predictions of vapor–liquid, liquid–liquid and vapor–liquid–liquid equilibria of fatty oil systems [31,32].

The GC-EOS routines, supported by Michelsen [33,34] minimization algorithm, were used to calculate pressure versus temperature phase envelopes at a given composition, as well as Gibbs' phase diagrams and equilibrium concentrations of the ternary (hydrogen + propane + sunflower oil) reactive mixture at different temperatures and pressures, which were also calculated using the same routines.

With these tools, the adequate working conditions could be selected and the evolution of each run could be followed during the whole reaction period. Homogeneity was experimentally confirmed, at every operating temperature and pressure.

The GC-EOS equation was also used to calculate the molar volumes of hydrogen, propane and the ternary mixture, at feed and reaction conditions. From these values and the total cell volume it was possible to calculate the number of moles of each component inside the reactor. The amount of hydrogen loaded into the cell was confirmed in an independent experiment, by checking the number of saturated double bonds in the oil, after all hydrogen had been consumed. A maximum difference of 3.5% was found between the calculated number of moles of hydrogen and the one derived from the analytical measurement.

Fig. 2(a) shows the calculated phase envelopes of three different isopleths with compositions equal to those of samples S1 (3.9% H_2), S3 (3.0% H_2) and S5 (1.6% H_2), taken at different reaction times during a hydrogenation experiment. The curves show a change from vapor–liquid (L_1V) to liquid–liquid (L_1L_2) equilibrium conditions, with a vapor–liquid–liquid (L_1L_2V) equilibrium point at the intersection of the L_1V and L_1L_2 lines. For each composition, the one-phase region is located above the corresponding phase envelope. Fig. 2(b) expands the low-temperature–low-pressure region of the diagram. The empty circles in Fig. 2 show the evolution of temperature and pressure inside the cell, during the heating and reaction processes. The cell was filled at 293 K under vapor–liquid equilibrium, and then, pressurized to reach homogeneous conditions. Hydrogen was consumed during the reaction, and the internal pressure in the cell dropped. The lines marked as S1–S5 represent the phase envelopes for the reaction mixture conditions. The circles numbered 1, 3 and 5 in the diagram show temperature and working pressure when the samples 1–5 were withdrawn. As shown in the figure, the reaction mixture remains in the one-phase region throughout all the process.

Fig. 3 shows the Gibbs' phase diagram for a working temperature of 374 K. The curves are the phase boundaries at the initial (16.7 MPa) and final (14.6 MPa) pressure of the cell. The markers represent the compositions of samples taken at

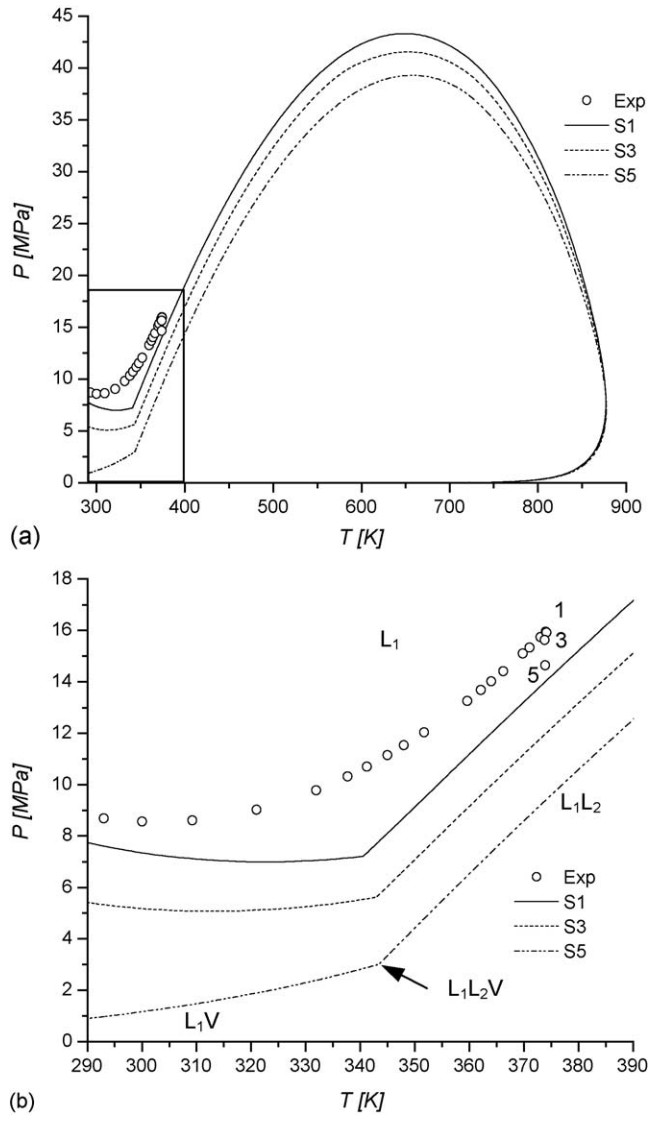

Fig. 2. (a) Phase envelopes of the reaction mixture for the samples 1, 3 and 5 (S1, S3 and S5 respectively). Hydrogen compositions in: S1, 3.9% H_2; S3, 3.0% H_2; S5, 1.6% H_2. (b) Zoom of the lower left corner indicated by the rectangle in (a). Empty circles numbered 1, 3 and 5 indicate the cell operating pressure the related samples were withdrawn at.

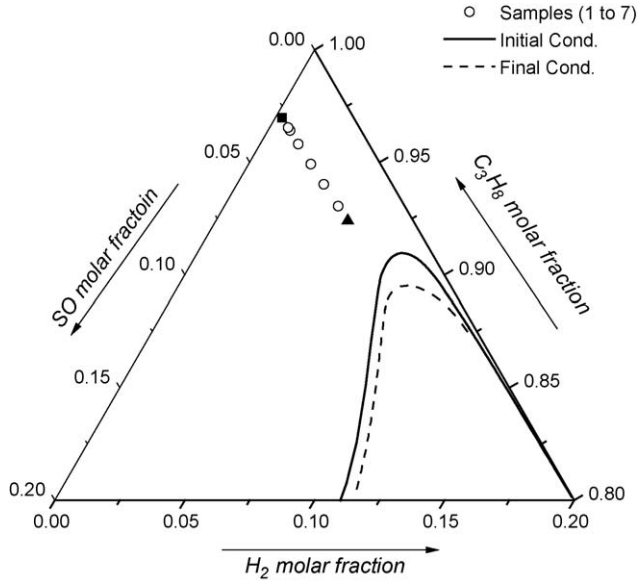

Fig. 3. Gibbs phase diagram at 374 K. Solid curve: phase boundary at 16.7 MPa. Dashed curve: phase boundary at 14.6 MPa. Data points indicate initial (Δ), intermediate (○) and final (■) compositions of the reactive mixture.

Table 1
Hydrogen chemisorption, AA and BET area results

Catalyst	Area [m^2/g]	% Metal	Dispersion	D_p [nm]
Pd-AN	9	0.86	0.26	4.2
Pd-AA	9	0.65	0.38	2.9
Pd-RGN	148	0.77	0.09	12.1
Pd-GN	148	0.77	0.29	3.9
Pd-GA	148	0.78	0.60	1.9

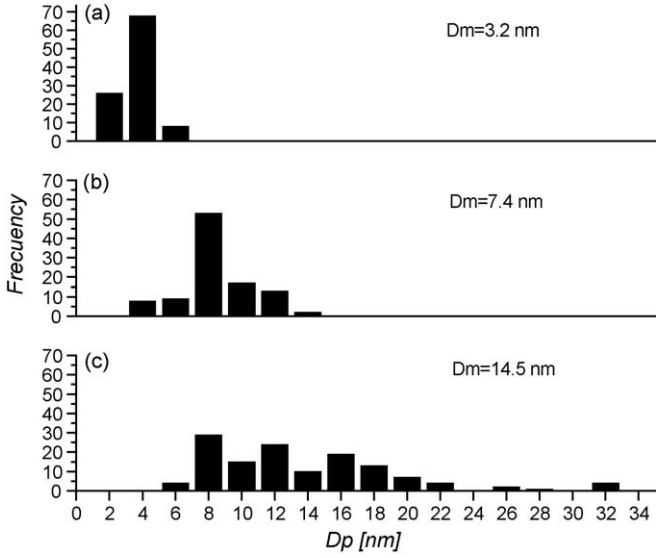

Fig. 4. Histograms obtained by TEM of the Pd-γ Al_2O_3 catalyst with different particle size: (a) Pd-GA, (b) Pd-GN and (c) Pd-GNR.

different reaction times. As hydrogen is consumed, the points approach the binary SO-C_3H_8. The initial and final samples have a hydrogen molar fraction equal to 5.1 and 0.3%, respectively. The homogeneous conditions predicted by the thermodynamic model were confirmed by visual observation.

3.3. Catalyst characterization

Hydrogen chemisorption, metal content and BET area results are shown in Table 1. The palladium particles' diameter was calculated from H_2 chemisorption data using Eq. (2), assuming semispherical particles and a density of surface atoms of 1.27×10^{19} Pd atoms/m^2. The latter is an average value considering the low Miller index planes [35,36].

$$D_p[\text{nm}] = \frac{1.12}{D} \tag{2}$$

In Eq. (2) D is the metal dispersion or the palladium-exposed fraction. The Pd-GA catalyst has the smallest particle size probably because of the high specific area of the support and the organometallic precursor that were used. Palladium acetylacetonate ($Pd(C_5H_7O_2)_2$) links the metal to the surface by a ligand exchange method very specific to the octahedral site of the alumina support, generating small PdO clusters, which after reduction produce the metal particle [37].

The series of Pd-GA, Pd-GN and Pd-GNR catalysts were analyzed by transmission electron microscopy, to determine the average size and range of the metallic particles. From the micrographs of these catalysts, it was observed that the size distribution was mono-modal. Fig. 4 shows the statistics of the particle-size distribution. The Pd-GA has a narrow center at

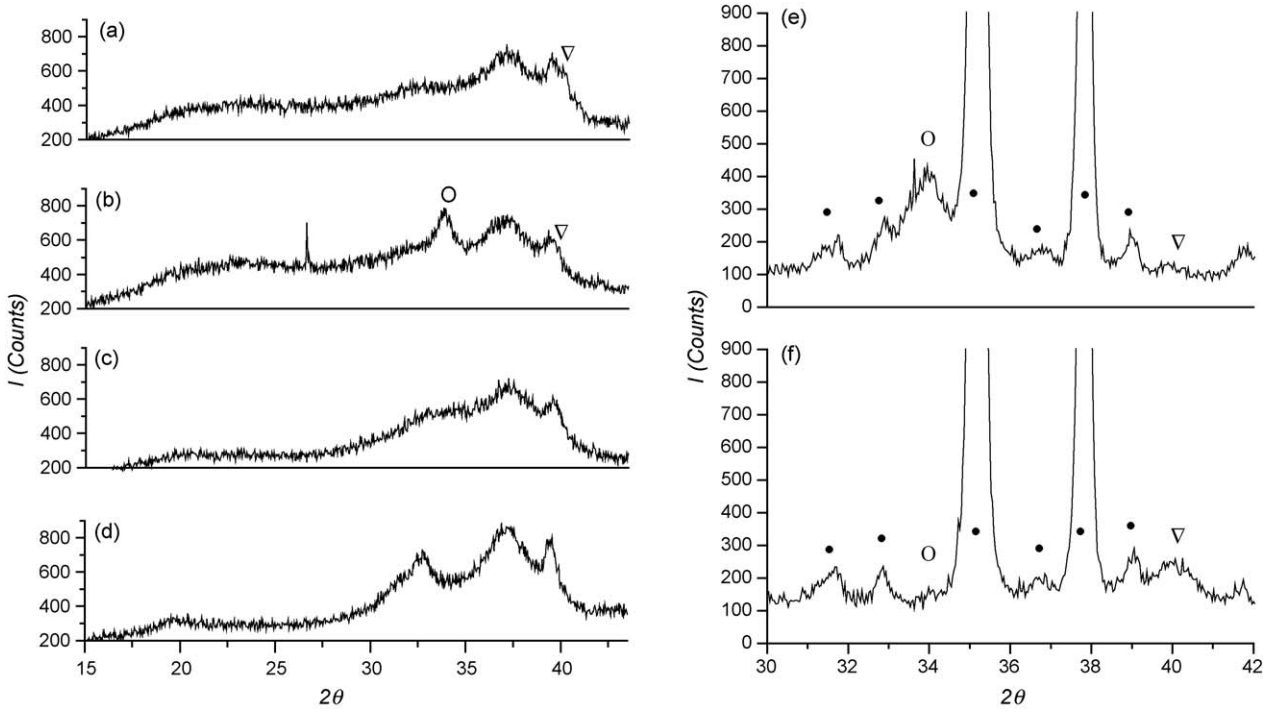

Fig. 5. XRD spectra of the Pd-γ Al_2O_3 catalyst with different particle sizes: (▽) Pd metallic; (○) PdO; (●) α-Al_2O_3. (a) Pd-GNR, (b) Pd-GN, (c) Pd-GA, (d) γ-Al_2O_3, (e) Pd-AN and (f) Pd-AA.

Table 2
Particle diameters of the catalysts PdG and PdA calculated from TEM and XRD measurements

Catalyst	D_{pTEM} [nm]	D_{pXRD} [nm]
Pd-GA	3.2	–
Pd-GN	7.4	6.6
Pd-RGN	14.5	10.6
Pd-AN	–	7.8
Pd-AA	–	3.6

3.2 nm. This value is greater than, almost twice as much as, the one calculated from H_2 chemisorption data. This could be attributed to the poor particle definition due to contrast problems and to the detection limit of the microscope (>2 nm). Pd-GN shows a broader distribution with a maximum at 7.4 nm and a tail reaching 14 nm (Fig. 4b). This is a consequence of the metal precursor used, which generates big size aggregates. Pd-GNR shows a very disperse distribution. Particle sizes, centered at 14.5 nm, are spread over a wide range (6–32 nm) (Fig. 4c). This indicates that a considerable growth of the supported particles occurred during the reduction treatment at 573 K [17].

Pd particle sizes were also determined from XRD analysis. No detectable peak for metallic Pd appears in Fig. 5c confirming the presence of small particles in the Pd-GA sample. Pd-GN (Fig. 5b) shows an important peak corresponding to PdO and another barely visible one corresponding to a metallic Pd. The reference peaks for the γ-Al_2O_3 used are shown in Fig. 5(d). Fig. 5(e and f) shows the XRD diagrams of Pd-α-Al_2O_3 catalysts, which differ from the previous ones because of the crystalline nature of the alpha phase. The peaks corresponding to Pd^0 and PdO are significant and are present in both diffractograms.

The deconvolution of the XRD signal, with a sum of Gaussian peaks with appropriate software, and the fixation of the corresponding peak to Pd^0 (1 1 1) and PdO at the particle size of the different samples ($2\theta = 40.115$ and 33.8, respectively) were calculated using the Scherrer approximation. The diameter thus obtained (Table 2) was compared with the one determined by H_2 chemisorption and TEM techniques. An overprediction of the TEM particle's diameters and fluctuating results from the XRD are evident. Due to the limitations of the physical techniques (detection limit, contrast between metallic particles and the support, minimum metal loading required to be detected, etc.), chemisorption data tend to provide more reliable information on average particle diameter, even though the relative uncertainty of the stoichiometric H/surface metal atom ratio adopted. For these reasons, the latter are assumed to be more representative. Botiaux et al. [38] report dispersion values for a series of catalysts of Pd supported in γ-Al_2O_3 using $Pd(C_5H_7O_2)_2$ as a precursor. For a metallic content of 0.76% reduced at 773 K, the dispersion value lies between 50 and 60%. Our results are in accordance with the tendency found by these authors.

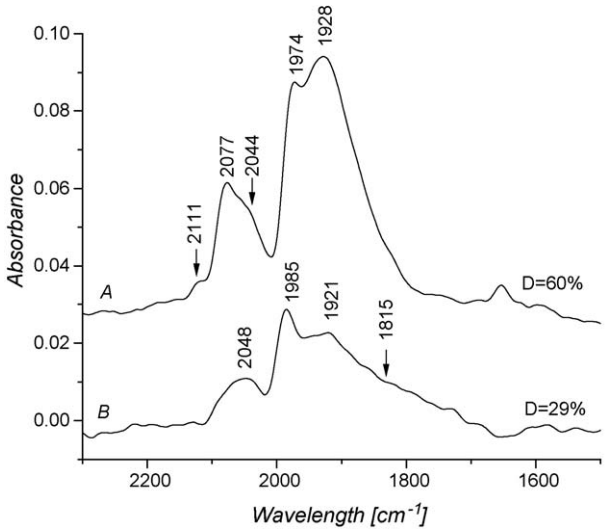

Fig. 6. IR spectra of CO adsorption over (A) Pd-GA and (B) Pd-GN catalysts.

The IR spectra of CO adsorption over Pd-GN and Pd-GA are presented in Fig. 6. The catalysts (30 mg) were calcined at 473 K and reduced at 373 K Pd-GA and 574 K Pd-GN. The spectra were recorded after 10 min with 2 Torr of CO.

The spectra show bands at frequencies ∼2080–2040 cm^{-1} associated with the linear CO adsorbed species and other two bands at ∼1980 and ∼1930 cm^{-1} associated with the bridged compressed and isolated species.

In Table 3, the ratio of linear/bridged peak area for both catalysts is presented. There is a shift of the linear band towards higher frequencies as dispersion increases. This reinforcement of the metal-CO bonding is due to the less back donation from Pd d orbitals [39]. The ratio between linear and bridged areas indicates the greater dispersion of the Pd-GA. The bridged

Table 3
Wavelength values and area peaks for the linear and bridged species for the catalysts Pd-GA and Pd-GN

Catalyst	Wavelength [cm^{-1}]		Area		Linear/bridged
	Principal peak	Deconvoluted peaks	Individual peaks	Total area	Area ratio
Pd-GA $\chi^2 < 5.10^{-6}$	2077	2111	0.41	2.2	0.253
		2077	1.17		
		2044	0.62		
	1974		0.47	8.71	
	1928		8.24		
Pd-GN $\chi^2 < 9.10^{-7}$	2048			0.84	0.168
	1985		0.50	4.99	
	1921	1934	3.00		
		1815	1.49		

species is notably different in both samples. The bands at ~1980 and ~1930 cm^{-1} were assigned to CO adsorbed on (1 0 0) and (1 1 1) Pd planes, respectively [40]. Fig. 6 shows that the Pd (1 0 0) band, corresponding to Pd-GN, moves at a higher wavelength than Pd-GA.

Making a deconvolution with a sum of Gaussian peaks, with a $\chi^2 < 5.10^{-6}$, the area and wavelength of each band could be assessed. They are reported in Table 3. The percentage of compressed bridged CO (Pd (1 1 1) plane) with respect to all multiply adsorbed species is 95% for Pd-GA and 60.5% for Pd-GN, respectively. There are two shoulders at both sides of the main band of the CO linear species on Pd-GA. The band at 2111 cm^{-1} could be assigned to Pd^+, the one at 2044 cm^{-1} to a linear species adsorbed on Pd^0 bulk, and the central band at 2077 cm^{-1} corresponds to CO adsorbed on small Pd^0 particles with low electronic density (between Pd bulk and Pd^+). The central band contributes to 49.5% of the total band area. This indicates the presence of small particles more electropositive than the Pd bulk according to Ref. [39]. Pd-GN presents a band at 1815 cm^{-1} (29.6% of the total bridged species) assigned to multiple coordinates of the CO species. This indicates the presence of well-developed planes on particles of large size.

3.4. Catalytic tests

A first set of reactions was carried out in a single-phase condition to search for the influence of the particle size effect upon the activity and selectivity using the Pd-GA, Pd-GN and Pd-GNR samples. The second set of reactions was conducted with the Pd-AA and Pd-AN catalysts to prove the influence of the support. Fig. 7(a and b) presents the Weisz–Prater (WP) module variation with the extent of reaction. The WP criterion evidences the magnitude of the mass transfer limitations [41]. Eq. (3) is the definition of this criterion, considering spherical particles where the δ (volume/external surface) relation is $D_p/6$.

$$\Phi_i = \frac{(-r_{OBSi})\rho_{cat}D_p^2}{36D_{effi}C_i} \quad (3)$$

In Eq. (3), C_i is the concentration of SO or H_2 [mol/m^3], D_{eff} the effective diffusion [m^2/s], D_p indicates the mean particle diameter [m], r_{OBSi} the observed rate of double bonds or H_2 consumption [mol/s kg_{cat}], and ρ_p is the apparent density of the catalyst [kg/m^3]. The SO and H_2 diffusion coefficients (1.10^{-9} and 1.10^{-7} m^2/s, respectively) were obtained from literature [15,42]. The catalyst density is 3750 kg/m^3 for Pd on γ-Al_2O_3 and 3790 kg/m^3 for Pd on α-Al_2O_3. The catalyst particle diameters were 211 and 225 μm for Pd on γ-Al_2O_3 and Pd on α-Al_2O_3, respectively. The tortuousness and porosity values of 4 and 0.5 were adopted. C_i was the corresponding concentration at each conversion level.

The WP criterion indicates that when $0.03 > \Phi_i$ (the difference between the surface and internal concentration for i is lower than 5%) there are no mass transfer problems for i, but complete mass transfer limitation occurs for $\Phi_i > 0.7$. The main variation Φ_i could be attributed to the variation of r_{OBS} and C_i. For the Φ_{H_2} values, C_i diminishes with conversion, but in the case of sunflower oil concentration it remains constant. All the Φ_{H_2} values for Pd-AN, Pd GN and Pd-GNR are below 0.03 most of the reaction time, but those of Pd-GA Pd-AA stay above this lower limit during all the reaction. All Φ_{H_2} values obtained (Fig. 7 b) are in the range $0.01 < \Phi_{H_2} < 0.05$. With Φ_{H_2} in this range, we suppose that H_2 is completely free of mass transfer problems considering that the criterion is an approximation. If there were some transport limitation, it would not be important enough to control the reaction. The

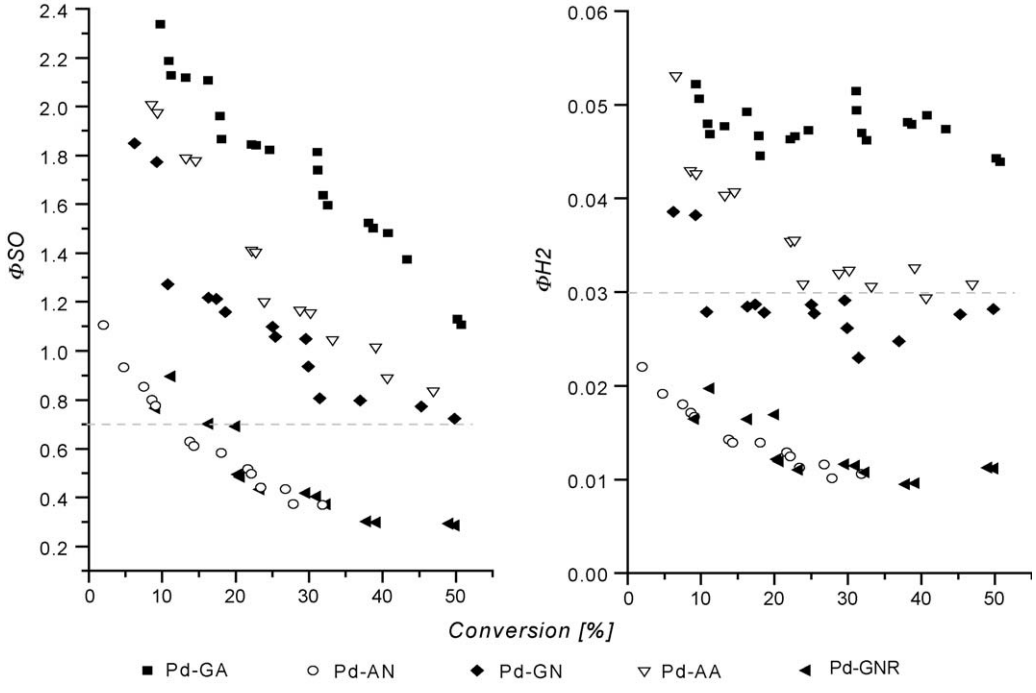

Fig. 7. Weisz–Prater module values against conversion during catalytic tests: (A) Weisz–Prater module for SO and (B) Weisz–Prater module for H_2.

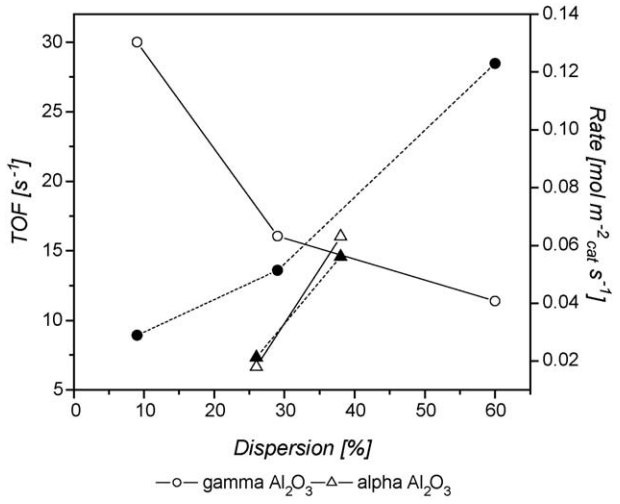

Fig. 8. Initial TOF and rates for the Pd-G and Pd-A catalysts. Empty symbols, TOF values; full symbols, rate values.

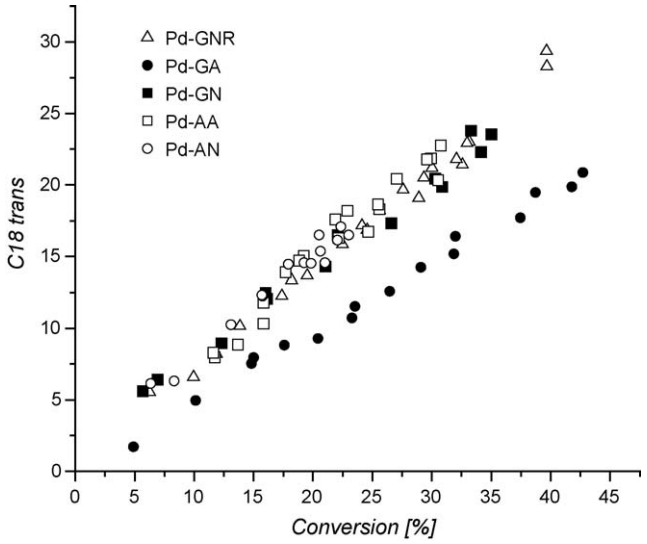

Fig. 9. *trans* Fatty acid content against total hydrogen conversion.

mass transport is greatly improved taking into account that $\Phi_{H_2} = 233.8$ and $\Phi_{SO} = 88.1$ for the conventional process carried out with the same catalyst [43].

The values of Φ_{SO} surpass the upper limit for all catalysts at the initial condition (Fig. 7a). Only Φ_{SO} for Pd-GNR and Pd-AN go down below $\Phi_i = 0.7$ at approximately 15% conversion. By reducing the mass transfer resistance; hydrogen is almost at the same concentration on the catalyst surface as in the fluid phase bulk. Furthermore, it is worth noting that external resistances to mass transfer are eliminated [1]. With this remark in mind, we speculate that the catalyst surface saturated of hydrogen, while on the other hand the surface lacks enough sunflower oil.

Fig. 8 shows the initial turnover frequency (TOF) and rates measured at 5% conversion as a function of the percentage of metal exposed (dispersion) for all the catalysts tested. For the Pd on γ-Al_2O_3 catalysts the TOF values decrease almost 2.7 times when the dispersion increases from 9 to 60% and the rate values increase at least 4 times in the same range of dispersion for the same metal content. Pd on α-Al_2O_3 catalysts shows an inverse tendency of the TOF values, where the rate values increase with dispersion. This behavior of the TOF values for the Pd on γ-Al_2O_3 series with small crystallites could be correlated to very strong adsorption of the diolefins on low coordination sites, whose proportion increases at high dispersion. The same was reported elsewhere [38,44] for the hydrogenation of 1,3-butadiene and 1-butyne. These authors use Pd catalysts supported in α and γ-Al_2O_3 and SiO_2 with palladium acetylacetonate and palladium tetramine nitrate ($[Pd(NH_3)_4]$ $(NO_3)_2$) as precursors. A decrease of 8 and 12 times was respectively found for the hydrogenation of 1,3-butadiene and 1-butyne when the dispersion increases from 20 to 100%. They attributed this behavior to the small particles and the way these hydrocarbons adsorb on low coordination sites, whose proportion increases at high dispersions. They associated this property of highly dispersed catalyst to the homogeneous catalyst, where the diolefin hydrogenation rate is often slower than that of the corresponding olefins, which can be interpreted by a stronger complexation of the metal by the highly unsaturated hydrocarbons. The same behavior is found in our results, with a decrease of almost 3 times of the TOF values for an increase of the dispersion from 9 to 60%. This discussion must take into account that our results concern molecules of MW = 870 g/mol and with a very complex spatial disposition. Furthermore, Ref. [38] reports that the TOF number does not change with the particle size for the butene hydrogenation, since both reactions occur consecutively (the butene hydrogenation begins when the 90% of 1,3-butadiene was consumed). In our case both di- and monounsaturated fatty acids are simultaneously converted, and a combined performance is expected. The decrease tendency indicates that the diene hydrogenation behavior prevails.

We cannot explain so far the behavior showed by the TOF versus dispersion of Pd supported on α-Al_2O_3.

To observe the selectivity to isomerization reaction, the total *trans* content was considered including the elaidic (C18:1 t) and the linolelaidic (C18:2tt, C18:2ct and C18:2tc) in the different position of the chain (i.e., 8, 10, 11, 13). This *trans* content is affected by the metallic particle size, as seen in Fig. 9. There is a marked difference between the Pd-GA, and Pd-GN (1.9 and 3.9 nm, respectively) samples. However, no significant difference is observed between Pd-GNR (with a particle size of 12.1 nm) from Pd-GN. Furthermore, no difference is detected between the Pd on α-Al_2O_3 catalysts and between the Pd-GN and Pd-AN, considering that they have similar Pd content and particle size, but with greater differences in specific area and support character.

Fig. 10(A) shows SR selectivity, defined as the ratio of the amount of total monounsaturated fatty acids (C18:1) formed with respect to the amount of diunsaturated converted (C18:2) [3]. Fig. 10(B) presents a formal way to characterize the saturated production [3]. This figure shows the amount of saturated fatty acids (C18:0) produced, as a function of the ratio of the amount of diunsaturated present to the initial

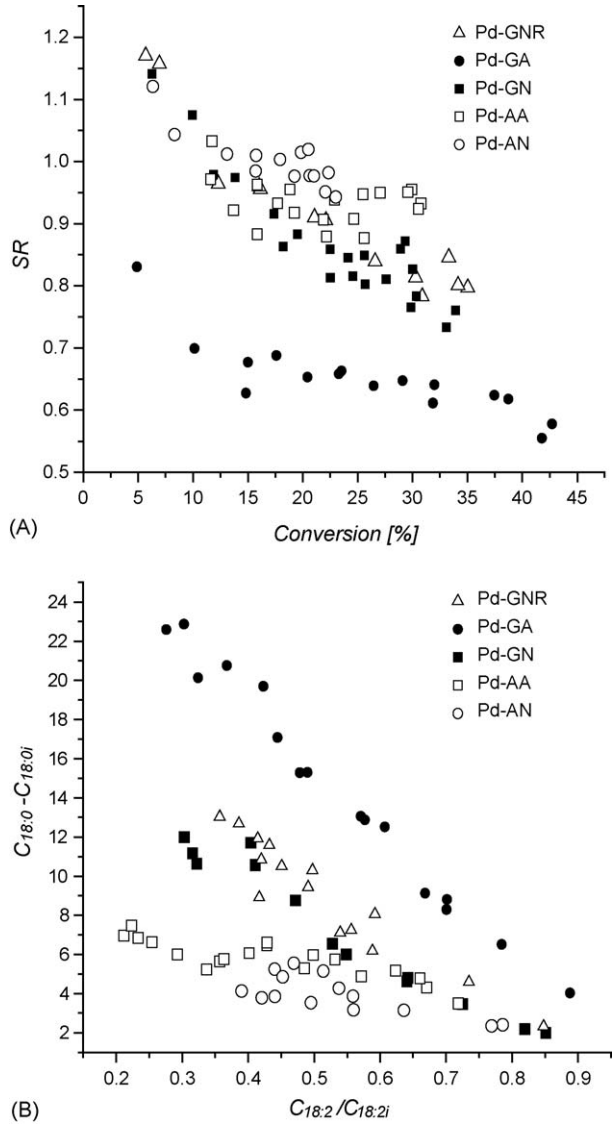

Fig. 10. (A) Selectivity ratio against total hydrogen conversion and (B) saturated production vs. linoleic consumption ratio.

concentration of diunsaturated (this is equal to the hydrogen conversion complement ($1 - x_{H_2}$)). From Fig. 10(B) a greater production of saturated chains for Pd-GA catalyst is observed, while no significant difference is detected for Pd-GN and Pd-GNR. According to Fig. 10(A), Pd-GA produces the lowest level of monounsaturated fatty acids, while the opposite is true for Pd-GN and Pd-GNR. Pd-AA remains in the tendency of the Pd-GN in both SR and saturated production, but Pd-AN shows a bigger amount of monounsaturated and a minor amount of saturated fatty acids than Pd-GN and Pd-GNR catalysts. Similar studies carried out at conventional conditions (P_{H_2} = 0.41 MPa, 373 K and 1400 rpm) in our lab with the same catalysts presented no difference in the *cis–trans* selectivity.

Both SR and saturated production selectivities are modified by the metallic particle size. The smaller particles favor the formation of saturated fatty acids, keeping the monounsaturated fatty acids at low levels. The particles of larger size present a greater tendency to form monoenes, probably

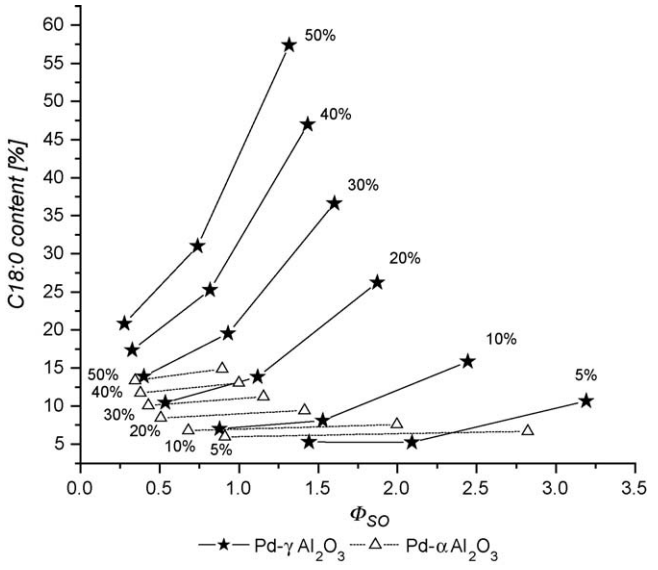

Fig. 11. Saturated content against Φ_{SO} for Pd-γ Al_2O_3 and Pd-α Al_2O_3 catalysts with conversion as parameter.

desorbing them before continuing with the hydrogenation to the saturation of the double bond. As shown in Fig. 9, the majority of these monounsaturated acids are in a *trans* configuration because it is more stable configuration in the thermodynamic sense. Taking into account the reaction path [45], these isomers can be produced by direct hydrogenation of dienes, or by geometrical isomerization of *cis*-monoenes [46]. Then, the result of low *trans* content is due to the larger saturation of the monounsaturated fatty acids. This fact can be attributed to diverse causes, for example, the sunflower oil mass transfer limitation founded for all catalysts (see Fig. 7a). In Fig. 11, the values of the saturated content as a function of the Weisz–Prater modulus for the sunflower oil are presented. The Pd on γ-Al_2O_3 catalysts show a growing sequence of saturated content with the increase of Φ_{SO}, this tendency increase with the reaction advance that is evidenced by the greater slope of the lines. This behavior is in accord with the reaction pathway, because when the catalytic surface is saturated of hydrogen the oil molecules that reach the active sites are hydrogenated to saturation rather than to desorbed in the monosaturated state. The Pd on α-Al_2O_3 series shows different behavior. The Φ_{SO} increase almost does not affect the saturated production. This is an abnormal performance; since both Pd-GA and Pd-AA have similar values of Φ_{SO} but the difference in the saturated content attain 3.8 times at 50% of conversion. Table 4 compares the values of rate, Φ_{H_2}, Φ_{SO}, H_2/Oil feed molar ratio and saturated production obtained by Ramirez et al. [47] in the hydrogenation of sunflower oil with supercritical propane with our values at similar conversions. The reaction of the Ref. [47] was carried out in flow regime (CSTR) with a commercial 2% Pd supported on activated carbon catalyst (Deggusa AG) and with a sunflower oil similar to the one used in this work (initial IV = 130). The value of the Φ_{SO} from the reference is 50 times greater than our values, while Φ_{H_2} is 10 times greater than those found here.

With the Φ_i values from the reference, the tendency to produce a saturated fatty acid is greater because Φ_{H_2} remains

Table 4
Φ_{H_2}, Φ_{SO} and saturated content. Values taken at for IV = 110. The definition of IV is found at elsewhere [3]

Catalyst	Rate [mol/g_{cat} s]	Φ_{H_2}	Φ_{SO}	Conversion [%]	H_2/oil feed molar ratio	Saturated production [%]
Pd-AC*	2.64×10^{-4}	0.7	69.9	25.2	10	14
Pd-GA	3.25×10^{-4}	0.045	1.25	25	2	23
Pd-GN	1.96×10^{-4}	0.028	0.8	25	2	15

* Values of the Ramirez et al. [47].

below the criterion limit (<0.7). According to their Φ_{SO} value, the oil suffered more severe problems to accede to the active sites than in our conditions. Furthermore, the H_2/Oil feed molar ratio used in the reference work is 5 times higher, which favors the saturate formation too. The saturate content for the Pd-GA is 64% larger than for the reference conditions and it is similar for Pd-GN catalyst in spite of the Φ_i values. This result indicates that some other factor, like the catalyst morphology, could influence the selectivity.

The behavior of Pd-GA could be explained by electronic properties of the metallic particles modified by support interaction. Some authors [48] reported a direct relationship between the electronic density and the particle size for the Rh supported catalysts, which has direct influence in the reaction rate and selectivity. The same phenomenon was observed for Pd and Pt catalysts [49]. According to Anderson [35], the changes in the electronic properties of the metallic Pd particles begin to be evident from 2 nm diameters, when the clusters possess fewer than 300 atoms. With the addition of metallic atoms to the cluster, the 5s-band is broadened and eventually overlaps the narrow 4d-band until the Pd bulk-band structure is generated. The smaller particles suffer an electronic deficiency. Roughly estimated a Pd-GA cluster contains 200 atoms and some interaction could be expected. For Pd-GN it becomes less probable because its metallic particles contain about 1400 atoms. Thus, the double-bond adsorption in small particles becomes stronger. This was evidenced by the IR spectrum of adsorbed CO, where the frequency corresponding to linear band shifts to higher wavelength (see Table 3) was reported [50–52]. Shifts in the CO adsorption signal to lower wavelengths when additives, like electronic donors (e.g., piperidine, CO and others), were incorporated to Pd, Pt and Rh supported catalysts. Likewise, these authors noticed shifts to higher wavelengths when electronic acceptors (e.g., *tert*-butyl chloride) were added.

In the 1,3-butadiene liquid-phase hydrogenation, Botiaux et al. [51,52] (using γ-Al_2O_3 with 97 m^2/g and 98% of dispersion) reported different catalytic activity and diverse selectivity to *trans*/*cis* 2-butene and *n*-butane when Pt was modified with an electronic donor or acceptor. In the first case—i.e., using piperidine as additive—Pt showed lower absorption wavelength in the FTIR measurements. The metal specific activity (TOF) decreased 47% with respect to the unaltered catalyst. At 72% conversion, the 1-butene and *n*-butane molar fractions were 50 and 23%, respectively. At this reaction advance, the *trans*/*cis* 2-butene ratios was 3.8. With *tert*-butyl chloride higher absorption wavelength in the FTIR measurements was observed than the reference catalyst's and the reaction rate was higher, but the TOF decreased in 23%. The 1-butene and *n*-butane molar fractions were 12.5 and 65%, respectively, at the same conversion value, where the *trans*/*cis* 2-butene ratio was 2.5.

The same behavior is found in the present work with small, medium and large particle sizes. It should be remarked that the adsorption constant of diunsaturated fatty acids is 4 times greater than for the monounsaturated ones in the conventional three-phase process [53].

Other authors [54] in the 1-3 butadiene hydrogenation found that the adsorption energy of the diunsaturated molecules should vary with the metallic particle size. They propose that larger particles of Pd (high electronic density) would disfavor *n*-butane and the 1-but-1ene formations, increasing the *trans*/*cis* 2 butene ratio. High electronic densities disfavor the carbene formation in this reaction.

For the Pd-GN catalyst, the diunsaturated fatty acid chain is adsorbed and hydrogenated, whereas the monoene tends not to remain adsorbed. On the contrary, in Pd-GA the monoene remains adsorbed or adsorbs from the bulk more strongly and the hydrogenation continues to the complete saturation. Were reported [55,56] that the direct hydrogenation from linoleic to stearic methyl ester (''shunt'' reaction) take place in the same order than the linoleic simple hydrogenation, when diffusion problems are absent. These differences are not present between Pd-GN and Pd-GNR catalysts, since both present particles would have similar electronic configurations corresponding to Pd bulk and sizes greater than 2 nm.

In addition, the Pd-AA and Pd-AN selectivity results have lower tendency to produce saturated fatty acids than those of Pd-GN. However, the metal size of Pd-AA is smaller and for Pd-AN has almost the same diameter. These facts show that, in some way, the support has an influence over the Pd clusters, enriching the electrons of the metal, increasing the electronic density.

This is true because the reaction is in lower level sensitive to the metal disposition when both reactants are more available.

4. Conclusions

Pd catalysts of particle sizes from 1.9 to 12.1 nm were used in the sunflower oil hydrogenation in single-phase medium. The Weizs–Prater criterion was applied to verify mass transport limitations. No transfer problems were found for H_2 and strong limitations were found for sunflower oil for all catalysts at the beginning of the reaction, but for some of them the transfer problem remains during all the reaction. The reaction seems to be sensitive to the metal particle size. The turnover frequency

decreases from 30 to 11.4 s^{-1} when the dispersion increases from 9 to 60%. The selectivities to the *trans*, monounsaturated and saturated fatty acids were found to be sensitive to the metal particle diameter. Larger particles favor the unsaturated and *trans* fatty acid formation, where small particles favor the saturated and low *trans* content. Both results are explained by the adsorption strength of the high-unsaturated fatty acids, which is modified by the particles size. Small particles favor the direct hydrogenation from linoleic to saturated products.

Acknowledgements

The authors would like to thank Dr. D. Vega and the Physics Department of Universidad Nacional del Sur (UNS) for their cooperation and Eng. C. Gigola, and I. Costilla for their contribution. Special recognition to the mechanical workshop R. Campello & Sons for the technical support. Thanks to Universidad Nacional del Sur and the Consejo Nacional de Investigaciones Científicas y Técnicas (CONICET) for the financial support.

References

[1] B. Fillion, B. Morsi, K. Heier, R. Machado, Ind. Eng. Chem. Res. 41 (2002) 697.
[2] I. Horiuti, M. Polanyi, Trans. Faraday Soc. 30 (1934) 1164.
[3] H.B. Patterson, Hydrogenation of Fats and Oils: Theory and Practice, second ed., JAOCS Press, Illinois, 1994, pp. 1–28.
[4] J. Booyens, C. Louwrens, I. Katzeff, Med. Hypotheses 25 (1988) 175.
[5] R. Mensink, M. Katan, N. Engl. J. Med. 45 (1990) 323.
[6] W. Willett, A. Ascherio, Am. J. Public Health 84 (1994) 722.
[7] G. Carturan, G. Facchin, G. Navazio, La Chim. E L'Ind. 65 (1983) 687.
[8] A. Wright, A. Mihele, L. Diosady, Food Res. Int. 36 (2003) 797.
[9] E. Draguez, D. Hault, A. Demolin, J. Am. Oil Chem. Soc. 61 (1984) 195.
[10] B. Nohair, C. Especer, G. Lafayea, P. Marécota, L.C. Hoangb, J. Barbier, J. Mol. Catal. A: Chem. 229 (2005) 117.
[11] M. Fernández, C. Piqueras, G. Tonetto, G. Crapiste, D. Damiani, J. Mol. Catal. A: Chem. 233 (2005) 133.
[12] A. Wright, A. Mihele, L. Diosady, Food Res. Int. 36 (2003) 797.
[13] A. Baiker, Chem. Rev. 99 (1999) 453.
[14] M. Macher, J. Högberg, P. Møller, M. Härröd, Lipid–Fett. 8 (1999) 301.
[15] M. Macher, Supercritical Hydrogenation of Vegetable Oils, Ph.D. Thesis, Chalmers University of Technology, Göteborg, Sweden, 2001.
[16] S. van den Hark, M. Härröd, Appl Catal A: Gen. 210 (2001) 207.
[17] L.W. Konopny, Preparación, Caracterización y Ensayo de Catalizadores de Pd-Mo Soportados en Gamma Alumina, Ph.D. Thesis, Universidad Nacional del Sur, Bahía Blanca, Argentina, 1996.
[18] A. Pisanu, C. Gigola, Appl. Catal. B 11 (1996) 37.
[19] J. Benson, H. Hwang, M. Boudart, J. Catal. 30 (1973) 146.
[20] S.J. Chen, R.E. Randelman, R.L. Seldomridge, M. Radosz, J. Chem. Eng. Data 38 (1993) 211.
[21] K. Anderson, M. Hell, L. Löwendahl, N. Scöön, J. Am. Oil. Chem. Soc. 51 (1974) 171.
[22] S. Pereda, S. Bottini, E. Brignole, AIChE J. 48 (2002) 2635.
[23] E. Straver, J. de Roo, C. Peters, J. de Swaan Arons, Supercritical engineering science: fundamentals and applications, in: ACS Symposim Series, E. Kiran, J. Brennecke (Eds.), 1994, p. 46.
[24] S. Bottini, T. Fornari, E. Brignole, Fluid Phase Equilib. 158 (1999) 211.
[25] P. Van Konynenburg, R. Scott, Philos. T. R. Soc. A 298 (1980) 495.
[26] P. Van Konynenburg, Discuss. Faraday Soc. 49 (1970) 87.
[27] H. Coorens, C. Peters, J. De Swaan Arons, Fluid Phase Equilib. 40 (1988) 135.
[28] S. Pereda, Ingeniería del Equilibrio entre Fases: Aplicación a Reactores de Hidrogenación Supercrítica, Ph.D. Thesis, Universidad Nacional del Sur, Bahía Blanca, Argentina, 2003.
[29] L. Rovetto, S. Bottini, E. Brignole, J. Supercrit. Fluids 25 (2003) 165.
[30] S. Skjold-Jørgensen, Fluid Phase Equilib. 16 (1984) 317.
[31] S. Espinosa, T. Fornari, S. Bottini, E. Brignole, J. Supercrit. Fluids 23 (2002) 91.
[32] L. Rovetto, "Equilibrio entre Fases en Procesos de Hidrogenación en Medios Supercríticos", Ph.D. Thesis, Universidad Nacional del Sur, Bahía Blanca, Argentina, 2004.
[33] M. Michelsen, Fluid Phase Equilib. 9 (1982) 1.
[34] M. Michelsen, Fluid Phase Equilib. 9 (1982) 29.
[35] J.R. Anderson, Structure of Metallic Catalyst, Academic Press, New York, 1975.
[36] P. Aben, J. Catal. 10 (1968) 224.
[37] E. Lesage-Rosenberg, G. Vlaic, H. Dexpert, P. Legard, E. Freund, Appl. Catal. 22 (1986) 211.
[38] J.P. Botiaux, J. Cosyns, S. Vasudevan, in: G. Poncelet, P. Grange, P. Jacobs (Eds.), Preparation of Catalysts III, Elsevier Science Publishers, Amsterdarm, 1983.
[39] M. Primet, J. Basset, M. Mathieu, M. Prettre, J. Catal. 29 (1973) 213.
[40] D. Tessier, A. Rakai, F. Bonzon-Verduraz, J. Chem. Soc. Faraday Trans. 88 (1992) 741.
[41] K.R. Westerterp, W.P. van Swaaij, A.A. Beenackers, Chemical Reactor Design and Operation, second ed., John Wiley Sons, New York, 1984 pp. 448–451.
[42] K.K. Liong, P.A. Wells, N.R. Foster, Ind. Eng. Chem. Res. 31 (1992) 390.
[43] M. Fernández, G. Tonetto, G. Crapiste, M. Ferreira, D. Damiani, J. Mol. Catal. A: Chem. 237 (2005) 67.
[44] J.P. Botiaux, J. Cosyns, S. Vasudevan, Appl. Catal. 6 (1983) 41.
[45] E. Santacesaria, P. Parrella, M. Di Sergio, G. Borrelli, Appl. Catal. A: Gen. 116 (1994) 269.
[46] A. Bernas, N. Kumar, P. Mäki-Arvela, N. Kulkova, B. Holmbom, T. Salmi, D. Yu Murzin, Appl. Catal. A: Gen. 245 (2003) 257.
[47] E. Ramírez, F. Recasens, M. Fernández, M. Larrayoz, AIChE J. 50 (2004) 1545.
[48] M. Ojeda, S. Rojas, M. Boutonnet, F. Pérez-Alonso, F. García-García, J. Fierro, Appl. Catal. A: Gen. 274 (2004) 33.
[49] M. Che, C.O. Bennett, Adv. Catal. 36 (1989) 55.
[50] M. Primet, J. Basset, M. Mathieu, M. Prettre, J. Catal. 29 (1973) 213.
[51] J. Botiaux, J. Cosyns, E. Robert, Appl. Catal. 49 (1989) 219.
[52] J. Botiaux, J. Cosyns, E. Robert, Appl. Catal. 49 (1989) 235.
[53] G.H. Jonker, Hydrogenation of edible oils and fats, Ph.D. Thesis, Rijksuniversiteit Groningen, Germany, 1999.
[54] A. Ramos, P. Silva Alves, D. Aranda, M. Schmal, Appl. Catal. 277 (2004) 71.
[55] R. Grau, A. Cassano, M. Baltanás, Chem. Eng. Sci. 5 (1988) 1125.
[56] R. Grau, A. Cassano, M. Baltanás, Catal. Rev. 30 (1988) 1.